Journal of Sound and Vibration 329 (2010) 43–55

Contents lists available at ScienceDirect

Journal of Sound and Vibration

journal homepage: www.elsevier.com/locate/jsvi

The effect of higher harmonic forces on fatigue life of marine risers

Y. Modarres-Sadeghi *, H. Mukundan, J.M. Dahl, F.S. Hover, M.S. Triantafyllou

Department of Mechanical Engineering, Massachusetts Institute of Technology Cambridge, MA 02139, USA

ARTICLE INFO

Article history:
Received 27 October 2008
Received in revised form
4 May 2009
Accepted 24 July 2009
Handling Editor: A.V. Metrikine
Available online 9 October 2009

ABSTRACT

Higher harmonic responses measured in flexible riser model tests conducted within the Norwegian Deepwater Programme (NDP) are studied to evaluate the effect of higher harmonics of force on the fatigue life of risers. A large third-harmonic contribution and sometimes a fifth-harmonic are observed for the majority of test cases. Since existing methods of fatigue life estimation account for the effect of hydrodynamic forces only at the frequency of vortex shedding, a new methodology is introduced which takes into account the influence of the higher harmonic components: First, a new response reconstruction technique is used to reconstruct the entire span-wise riser motion in both the cross-flow and in-line directions based on measurements at specific points along the length. Then, a force database obtained from forced in-line and cross-flow motions of rigid cylinders is used to estimate the higher harmonic components of the force along the entire riser length. A significant decrease in fatigue life is obtained when the higher harmonic components of the fluid forces are considered.

1. Introduction

The vortex-induced vibration (VIV) of long, flexible cylinders, such as marine risers and mooring lines, constitutes an important problem in deep water oil exploration and production. In particular, sustained vibration of risers can lead to structural failure due to fatigue damage; hence it is essential to accurately predict their fatigue life.

In an effort to understand the basic mechanisms of riser vibration, simpler problems were considered first. In particular, the vortex-induced vibration of short rigid cylinders has become the canonical problem for bluff body-flow interaction, and has been studied extensively. Recent reviews by Sarpkaya [1] and Williamson and Govardhan [2] outline the extensive sets of studies on rigid cylinder VIV; Vandiver [3] gives a review of flexible cylinder studies.

Previous studies of rigid cylinder VIV have focused on the cross-flow oscillation of the cylinder (motion perpendicular to the flow direction), neglecting the smaller in-line oscillations (motions parallel to the flow direction). This simplification has led to fatigue prediction methods for long flexible cylinders, such as risers, that are based on rigid cylinder vibrations with the cylinder allowed to move in cross-flow motion only. Recent studies have shown [4,5] that even for rigid cylinders, in-line oscillations cause drastic changes in the wake and the resulting fluid forces, including a significant third and in some cases fifth harmonic components in the measured cross-flow fluid force signals. The higher harmonic components have been observed in flexible risers as well, as shown in strain measurements on long flexible risers in a sheared ocean current [6].

Jhingran and Vandiver [7] incorporated the higher harmonic strain components in fatigue calculations for a series of experimental data by using the measured signals at discrete points along the length of the riser. The aim here is to go one step further and consider higher harmonic forces in fatigue life estimates using experimental data over the entire length of

* Corresponding author.
E-mail address: modarres@mit.edu (Y. Modarres-Sadeghi).

0022-460X/$ - see front matter © 2009 Elsevier Ltd. All rights reserved.
doi:10.1016/j.jsv.2009.07.024

Table 1
Physical properties of the NDP riser.

Outer diameter (D)	0.027 m
Length (L)	38 m
Mass per unit length (m)	0.933 kg/m
Displaced water/length (m_a)	0.576 kg/m
Mean tension (T)	4000–6000 N
Modulus of elasticity (E)	2.25 GPa

the riser, including points where measurements were not made. A novel procedure is used to reconstruct the response over the entire riser length.

A series of experimental data from the Norwegian Deepwater Programme (NDP) tests [8,9] are used to investigate the existence of these higher harmonic components in strain and acceleration signals measured on risers subjected to both uniform and linearly sheared flow profiles. In these experiments, strain and acceleration measurements have been conducted at a number of points along the length of the riser. These measurements can be used to obtain riser's orbital motion and also the fluid forces acting on the riser at the measurement points, and also the higher harmonic components of the signals.

First, a reconstruction of the entire motion of the riser is necessary in order to estimate fluid forces at points where measurements were not obtained. A new reconstruction method [10] is used. Then, employing a strip theory assumption, fluid forces are estimated along the length of the riser based on a force database obtained from forced cross-flow and in-line motion of rigid cylinders [11]. This provides an estimate of higher harmonic forces along the length of the riser and hence the fatigue life can be estimated continuously along the length of the riser; and therefore, the location of minimum fatigue life (or maximum fatigue damage) can be determined. Fatigue damage calculations are shown for several NDP experimental cases to assess the validity of the presented method.

2. NDP experimental data

We used the experimental data from the Norwegian Deepwater Programme (NDP) Riser High Mode VIV tests [8], which comprise uniform flow cases, where the flow velocity is constant along the riser and varies from U=0.3 to 2.2 m/s with 0.1 m/s steps in various test cases; and linearly sheared flow cases, where the flow velocity is zero at one end and increases linearly along the length, with maximum flow velocity varying from U=0.3 to 2.2 m/s with 0.1 m/s steps. Physical properties of the riser used in the experiments are given in Table 1. The model riser was taut horizontally and towed at various speeds, producing either uniform flow profiles if the two ends were towed at the same speed, or linearly sheared flow profiles if one end was fixed and the other end was towed. Measurements at 40 points were made of the in-line strain along the length, 24 measurements of the cross-flow strain, and eight measurements of the in-line and cross-flow accelerations. There are eight points along the length with measurements of both strain and acceleration, and in both cross-flow and in-line directions. The experiments were conducted on bare risers as well as risers with varying strake coverage.

3. Riser orbital motions and excitation region

The riser response data are not temporally statistically stationary; in fact, the response is observed to switch suddenly from one pattern of response to another. However, there are data segments consisting of dozens of cycles which are stationary. First, we establish the stationary segments [10] and all subsequent calculations are conducted over such segments. Fig. 1 shows a sample measured acceleration signal and the choice of a statistically stationary region.

The orbital motion of the riser at every point where acceleration measurements were obtained was calculated. The response is not purely sinusoidal and the orbits vary from cycle to cycle (Fig. 2); hence we chop the signal into sub-intervals, from one cross-flow up-crossing point to the next. This segment corresponds to two periods of the in-line oscillation. The orbital plot of the motion shows either a figure-eight or a crescent like motion (see Fig. 3). Using such sub-interval plots of the signals provides a much sharper picture of the nature of the response over short periods of time. Also the direction of motion of the riser orbit for each sub-signal can be found by calculating the phase difference between the cross-flow and the in-line displacements.[1]

Based on the orbit or the calculated phase differences, the motion is characterized as clockwise or counterclockwise; counterclockwise is defined when the riser is at the top of its trajectory and moving upstream with the cross-flow from left

[1] The short period considered in each sub-signal makes it possible to assume that the signal is sinusoidal. Therefore, one can assume:

$$y = Y\sin(\omega t)\; x = X\sin(2\omega t + \psi)$$

where ψ can be obtained by measuring the time difference between the cross-flow displacement zero up-crossing (the first point in each sub-signal) and the following in-line displacement zero up-crossing (δ). Once this is measured, the phase difference can be calculated as $\psi = 2\times(2\pi/\delta)(\Delta t)$, where $\Delta t = t_{final} - t_{initial}$ in each sub-signal.

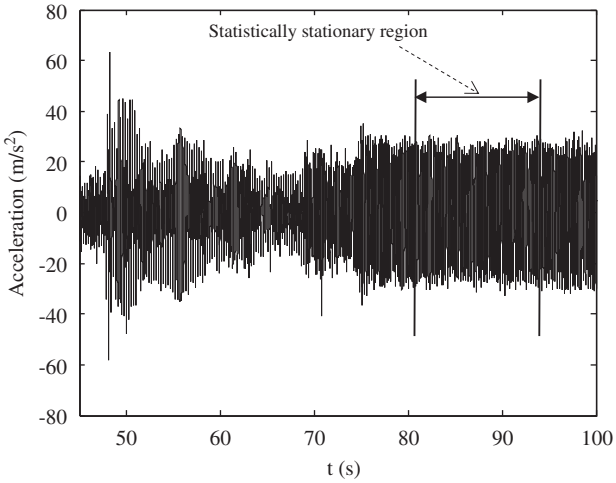

Fig. 1. A sample acceleration signal and its statistically stationary region.

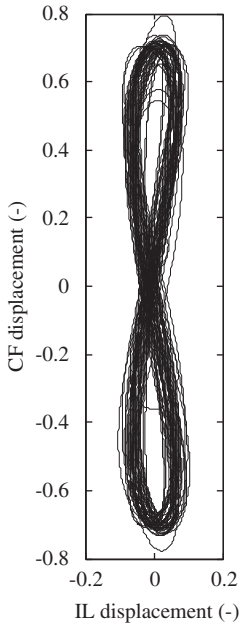

Fig. 2. A sample motion trajectory of the whole signal plotted in one figure.

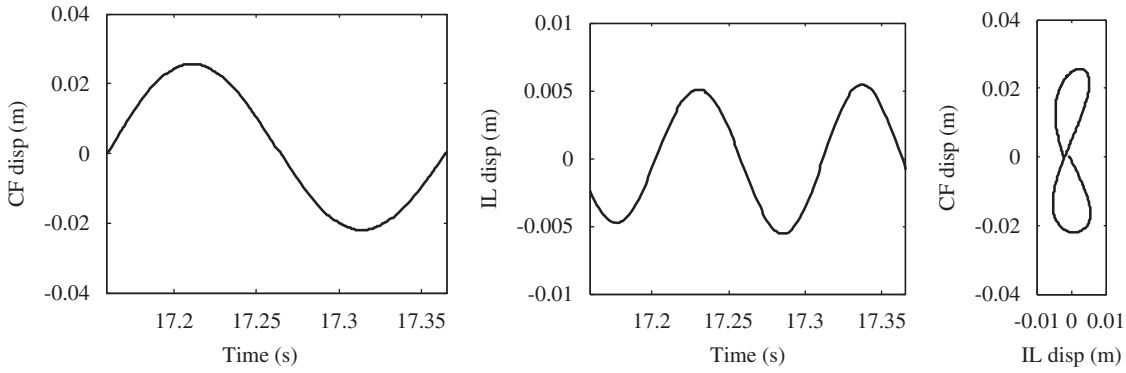

Fig. 3. The signal is cut such that every cross-flow displacement sub-signal contains only one period (two periods of the in-line displacement).

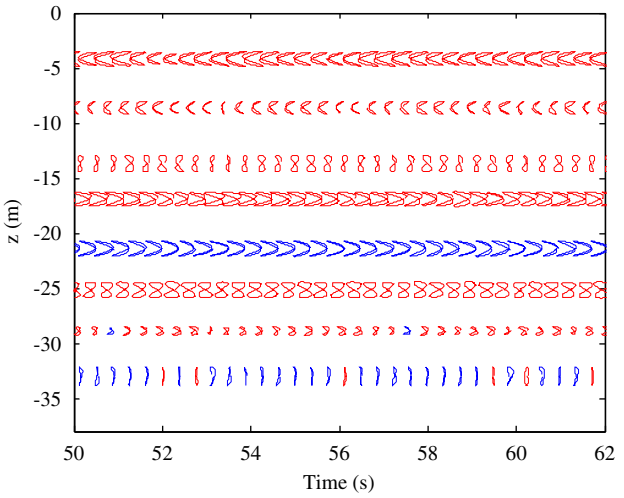

Fig. 4. Trajectories of sub-signals of a linearly sheared case with U_{max}=0.6 m/s over the statistically stationary range. Red: counterclockwise; blue: clockwise motion. The flow is left to right. (For interpretation of the references to color in this figure legend, the reader is referred to the web version of this article.)

to right. An example for a linearly sheared current case with the maximum flow velocity of 0.6 m/s is shown in Fig. 4 (maximum flow is at z=0). The riser's motion at each point along the length and at each time is given in color-coded plots, where blue indicates clockwise motion and red specifies counterclockwise motion. It is observed that the counterclockwise figure eight motions are observed mainly in the region with high local flow velocity. Similar counterclockwise motions have been observed for a freely vibrating rigid cylinder when the in-line natural frequency is roughly equal to twice the natural frequency in the cross-flow direction [5].

The excitation region can also be estimated for risers subjected to linearly sheared flow. As defined here, the region under excitation is the region for which $f^*=fD/U$, (where f is the principal frequency of vibration) is in the neighborhood of f^*=0.17, which corresponds to the region of maximum energy transfer from the flow to the structure. Here, $f_1^* = 0.1$ and $f_2^* = 0.25$ have been considered as the limits for estimating the excitation region.[2] It is observed that the excitation region of the riser includes the points which display counterclockwise figure-eight motions in linearly sheared flow cases. This behavior is consistent for all the sheared flow cases in NDP experiments.

4. Higher harmonic strain and acceleration components

In the majority of NDP signals, if the fundamental frequency of oscillation for the cross-flow strain and acceleration signals is denoted by f_{CF}, a peak at three times this frequency, i.e. around $f_{3CF}=3f_{CF}$ is also observed. Fig. 5 shows a sample PSD plot for an acceleration signal of one of the uniform flow cases with U=1.3 m/s. The fundamental frequency is at $f_{CF}\approx 7$ Hz, which is in the neighborhood of the expected Strouhal shedding frequency, $f=USt/D\approx 8$ Hz. A large third harmonic peak exists at $f_{3CF}\approx 21$ Hz$=3f_{CF}$ and a rather smaller one at $f_{5CF}\approx 35$ Hz$=5f_{CF}$. The main frequency in the in-line direction is around $f_{IL}=2f_{CF}$, as expected. The contribution of higher harmonic components in the transverse direction is determined by evaluating the ratio of the area under the higher harmonic peak in the PSD plot over the total area under the PSD. For example, in Fig. 5, if the areas under the third-harmonic and the fifth-harmonic peaks are denoted by A_3 and A_5, respectively, then the ratios A_3/A_{Total} and A_5/A_{Total} are the measures of the relative importance of these higher harmonic components, where A_{Total} is the total area under the PSD.

The higher harmonic components in the strain and acceleration signals can be calculated for all the test cases based on the discrete measurements of strain and acceleration. Fig. 6(a) shows plots of the relative third harmonic components magnitudes along the length of the riser for each uniform current case, based on acceleration signals. A total of twenty test cases (every 0.1 m/s step in horizontal axis) are included. A third harmonic component as large as 70 percent of the total acceleration can be observed in some cases, whereas a third harmonic component of around 0.5 (50 percent) is widely observed. Fig. 6(b) shows a similar plot for linearly sheared cases where the third harmonic components of acceleration are shown as a function of the maximum flow velocity U_{max} (U_{max} is at z=0). Again, third harmonic components are significant; however, overall they are not as large as third harmonics in uniform flow cases. The third harmonic contribution is mainly

[2] In a linearly sheared flow case, the dimensionless frequency is zero at the maximum z (zero flow velocity) and varies linearly as z decreases (flow velocity increases). The points along the riser whose corresponding dimensionless frequencies are equal to f_1^* and f_2^* are then calculated as $L_1=LU_1/U_{max}$ when $U_1 = fD/f_1^*$ and $L_2=LU_2/U_{max}$ when $U_2 = fD/f_2^*$. Then, the excitation region can be found as $\Delta L=L_1-L_2$.

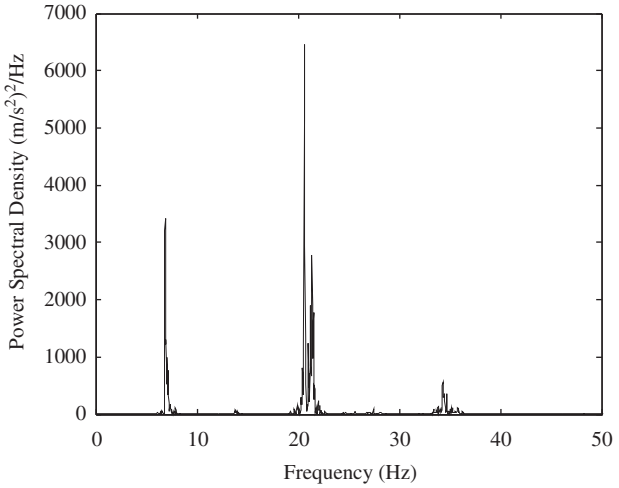

Fig. 5. A typical PSD plot of a measurement point with a large peak at the third harmonic (around 21 Hz) and a small peak at the fifth harmonic (around 35 Hz).

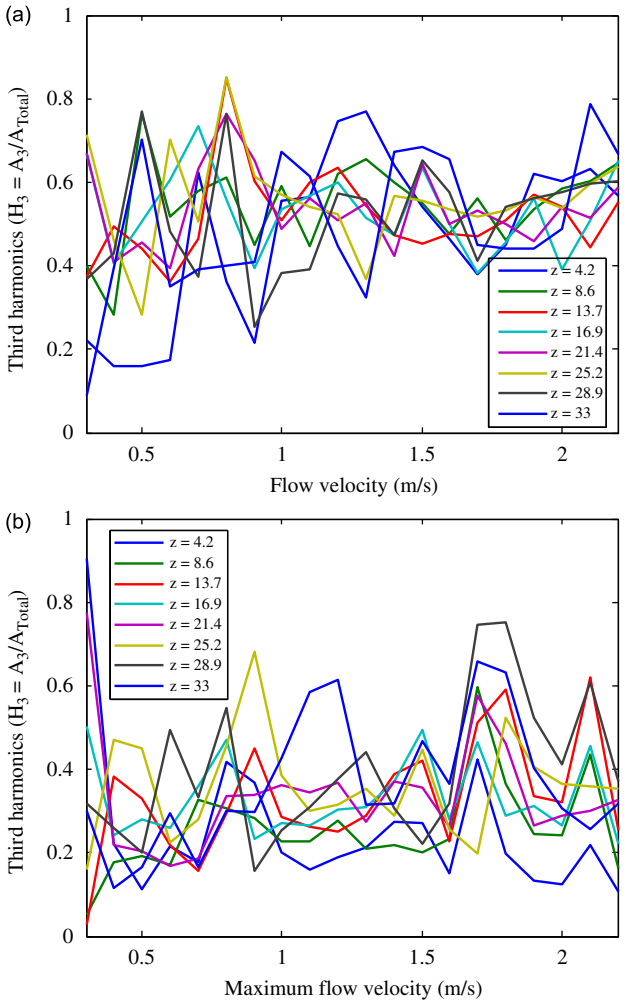

Fig. 6. Third harmonic components (H_3=A_3/A_{Total}, as defined in Section 4) of the statistically stationary region of acceleration signals along the length for (a) uniform current and (b) linearly sheared current of the NDP cases versus the (maximum) flow velocity. Similar patterns are observed for higher harmonic components calculated based on strain signals. (For interpretation of the references to colour in this figure legend, the reader is referred to the web version of this article.)

around 30–40 percent with some exceptional points where a relatively large contribution of up to 80 percent can be observed. As will be seen later, the influence of a third harmonic of around 0.3 (30 percent) on fatigue life is enough to be non-negligible. Similar plots for the fifth harmonic components (not presented here) show a contribution of mainly 15–20 percent both for the uniform and the linearly sheared cases, with some cases of the fifth harmonic up to 30 percent. The higher harmonic contributions can be calculated in a similar manner using the measured strain signals, resulting in plots similar to those of Fig. 6 with similar values for higher harmonics.

5. Response reconstruction

A method has been developed [10] to reconstruct the VIV response of a long flexible cylinder using data from limited number of sensors (typically strain gauges and accelerometers) placed along its length. When the number of sensors (N_s) is sufficient (namely, $N_s \geqslant 2N_m+1$, where N_m is the number of spatial harmonics), the problem of reconstructing the riser VIV response can be posed as a spatial Fourier decomposition. The displaced shape of the riser at any instance of time is written as a spatial Fourier series, in terms of both the sine and cosine terms. The reconstruction problem is posed as a system of linear equations, where the unknown spatial Fourier coefficients at every instance of time are evaluated. Since the number of sensors is larger than the critical number, this is an over-determined system of linear equations. This system is solved using a pseudo-inverse, where the least square error is minimized. This method allows estimation of the continuous motion of the riser (at every point along its length) and therefore fatigue life estimation is not limited to only the measurement points.

There are three main sources of uncertainties in this reconstruction method: (i) uncertainty due to the presence of noise in experimental data, (ii) uncertainty due to the use of limited number of sine and cosine terms, and (iii) uncertainty due to the presence of both acceleration and strain measurements. Due to these uncertainties, the amplitude of reconstructed response at every point along the length will have an upper bound and a lower bound (see [10] for a detail discussion).

This method can be used to reconstruct riser displacements mainly based on the first harmonic component of VIV. Reconstructing the third harmonic components requires data from three times the number of sensors required for reconstructing the first harmonic components, which is normally unavailable. The number of required sensors for reconstruction increases with increasing flow velocity, and therefore increasing frequency of excitation. Thus for scenarios involving lower flow velocities, the third harmonic components can be reconstructed (as the number of existing sensors is enough), but not for cases with larger flow velocities. As a result, in this paper we use the reconstruction method to get a continuous figure of riser motion only based on the fundamental VIV frequency. Then, we use other methods, as discussed in the following sections, to include the influence of higher harmonics.

6. Force database for rigid cylinders

The reconstructed response of the riser contains only the first harmonic components of acceleration and strain. Third harmonic hydrodynamic forces have been shown to be a function of the relative motion of shed vortices with respect to the cylinder motion [11]. These third harmonic hydrodynamic forces can therefore be present even in the absence of third harmonic cylinder response. In order to account for higher harmonics, we first assume a strip theory representation of the riser such that the hydrodynamic forces acting at a particular point along the riser are equal to the forces on a rigid cylinder with equivalent orbital response (same cross-flow and in-line amplitudes and phase between cross-flow and in-line motion). Reduced velocity, defined as $V_r=U/fD$, where U is flow velocity, f is frequency of oscillations and D is cylinder diameter, is matched as well to ensure similar flow kinematics around the riser segment.

Hydrodynamic force estimates are obtained from forced cylinder motions in experiments conducted at the MIT Towing Tank [11]. In the experiments, a rigid cylinder is forced to move in various combinations of cross-flow (Y) and in-line (X) amplitudes at various reduced velocities. The phase between in-line and cross-flow motions is varied as well, producing a database of 2304 possible motion combinations. Lift and drag forces are measured for each cylinder motion. For an individual reduced velocity, the varied amplitudes and phases create a 3-D array. The data from [11] at V_r=6.5, for example, show that the third harmonic almost always increases with increasing in-line amplitude. In this region, the third harmonic remains almost constant, with fairly low magnitude. The values only become large with large in-line amplitudes. This is expected since we know that the third and the fifth harmonics are a direct result of the relative velocity change between shed vortices and the cylinder motions caused by in-line motions. This rigid cylinder force coefficient database is used to estimate the higher harmonic components of riser's motion as will be discussed in detail in the following section.

We ought to mention here that this rigid cylinder database has some limitations: It covers a wide parametric range and hence, although consisting of 2304 tests, it is relatively sparse and this requires that the database be interpolated to determine intermediate values. Also, these tests were conducted at a Reynolds number Re=8800, which differs from the NDP tests. In the present work, we have not tried to correct the results for the difference in Reynolds numbers. However, it should be mentioned that for subcritical Reynolds number, below typically Re=250,000, the influence of Reynolds number is mild and does not change the basic features of the vortex induced response.

7. Higher harmonics estimation

As discussed in Section 5, by using the measured signals in the cross-flow and in-line directions, we can reconstruct the riser's motion in two perpendicular directions and therefore we can calculate the cross-flow and in-line magnitudes, as

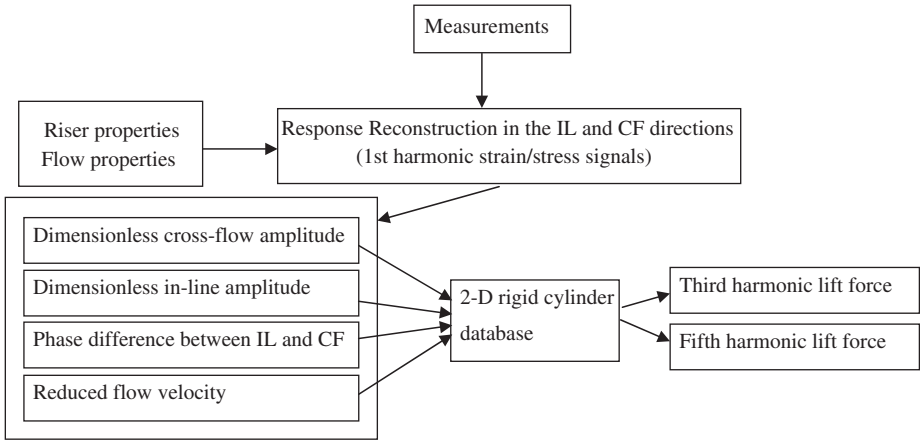

Fig. 7. Flowchart of the method used to estimate the higher harmonics of riser response based on the continuous response reconstruction and by using the forced 2-D rigid cylinder database.

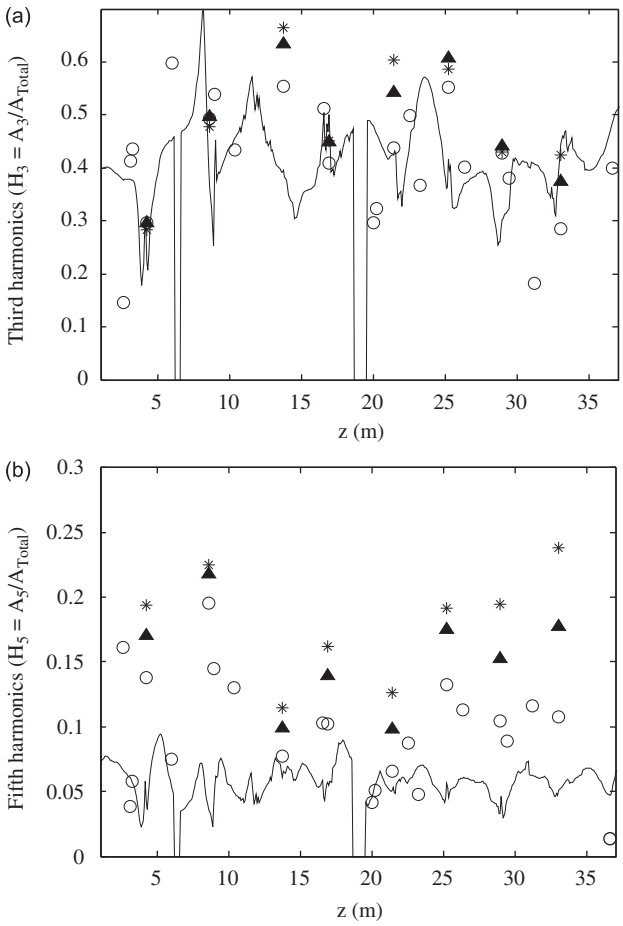

Fig. 8. (a) Third harmonic components (H_3=A_3/A_{Total}, as defined in Section 4) and (b) fifth components (H_5=A_5/A_{Total}, as defined in Section 4) of force predicted using the rigid cylinder database (continuous line) and those calculated from the measured acceleration (∗) and strain (○) signals and estimated force (▲) for a uniform flow case with U=0.8 m/s.

well as their phase difference at each point along the riser. Then, we assume every segment of the riser is a rigid cylinder for which we know the cross-flow and in-line magnitudes, the phase difference and the flow velocity. With these data, we can use the 2-D rigid cylinder database and interpolate the higher harmonic components of force. Fig. 7 gives a summary of this methodology in a flowchart. We have applied this method to some NDP test cases and Figs. 8 and 9 show the results for two sample cases: For a uniform flow profile and for a linearly sheared flow profile. In each of these figures, the upper plot corresponds to the third harmonic components and the lower plot corresponds to the fifth harmonic components. The continuous lines correspond to predictions based on the reconstructed motions and using the data from the 2-D rigid cylinder database. This is done following the procedure depicted in Fig. 7. The specific higher harmonic components of hydrodynamic force are interpolated from the rigid cylinder database in order to obtain the force distribution along the length of the riser, based on the in-line and transverse motions at each point along the riser. In cases where the interpolation point is out of range of the rigid cylinder database, a zero higher harmonic is estimated. This is the case, e.g. at $z \approx 6$ m and $z \approx 19$ m for the uniform flow case (Fig. 8). In the sheared flow case (Fig. 9), the reduced velocities for $z > 17$ m are smaller than the minimum reduced velocity tested in the 2-D rigid cylinder tests, and therefore are omitted here.

At points where measurements are available, the higher harmonics can be calculated directly from the measured signals. These points are used as a measure for the validity of our estimated higher harmonics, and are plotted in Figs. 8 and 9 as symbols. It should be mentioned here that the higher harmonic components calculated directly from the measurement points are based on acceleration (asterisks in the figures) or strain (circles in the figures) signals, while the higher harmonic components interpolated from the rigid cylinder database are force higher harmonics (calculated based on lift force signals) and therefore, they cannot be necessarily compared directly. In order to be able to do a direct comparison, we need to calculate the force based on the measured strain and acceleration signals. At points where both acceleration and strain measurements are available, with neglecting the structural damping and the bending stiffness, the force can be calculated as

$$m_T \ddot{y} - T y'' = F_v, \tag{1}$$

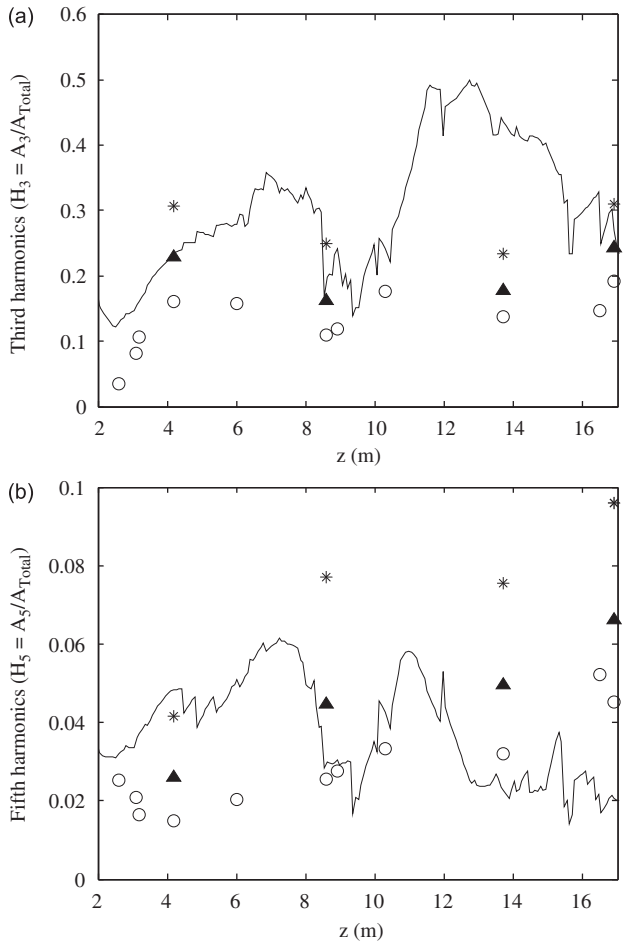

Fig. 9. Same plot as Fig. 8 for a linearly sheared flow case with U_{max}=0.8 m/s, where U_{max} is at z=0.

where m_T=m+m_a=1.509 kg/m, T=5000 N and F_v is the fluid force minus the nominal added mass force. To show that the bending stiffness is negligible compared to the tension stiffness, we form the ratio of the two restoring forces as expressed by e=$EIn^2/(TL^2)$, where E is Young's modulus, I the moment of inertia, L the riser length, T the mid-point tension and n the mode number excited, and we find $e \approx 5 \times 10^{-6} n^2$, clearly indicating that the bending stiffness is small, even for large mode numbers (for n=20, which is a large mode number in the NDP experiments, we find $e \approx 0.002$). The higher harmonics predicted based on this estimation of the force are also shown in Figs. 8 and 9 (triangles) and can be directly compared with the continuous lines. Overall, the predicted higher harmonic components are reasonably close to the ones calculated directly from the experimental measurements.

What we need later on in our fatigue calculations is the higher harmonic components of the strain signal. However, the higher harmonic components that are interpolated from the rigid cylinder database are those of force. In what follows, we assume that we can use strain higher harmonics and force higher harmonics interchangeably. The results shown in Figs. 8 and 9 are in favor of this assumption, as the higher harmonic components of force (triangles) are close to the higher harmonic components of strain (circles), at least at the measurement points.

Fig. 10 shows the predicted (circles) and measured (asterisks) higher harmonic components of force for a point at $z \sim 4$ m, as an example, for 14 uniform and 14 sheared flow cases. For these cases, the flow velocity (constant for uniform flow cases and maximum for linearly sheared flow cases) varies from 0.6 to 1.9 m/s. The same trend is observed in variation of the third harmonic component versus case number for both predicted and measured values, which shows that our prediction method reflects the differences from one case to another, consistent with the measured values.

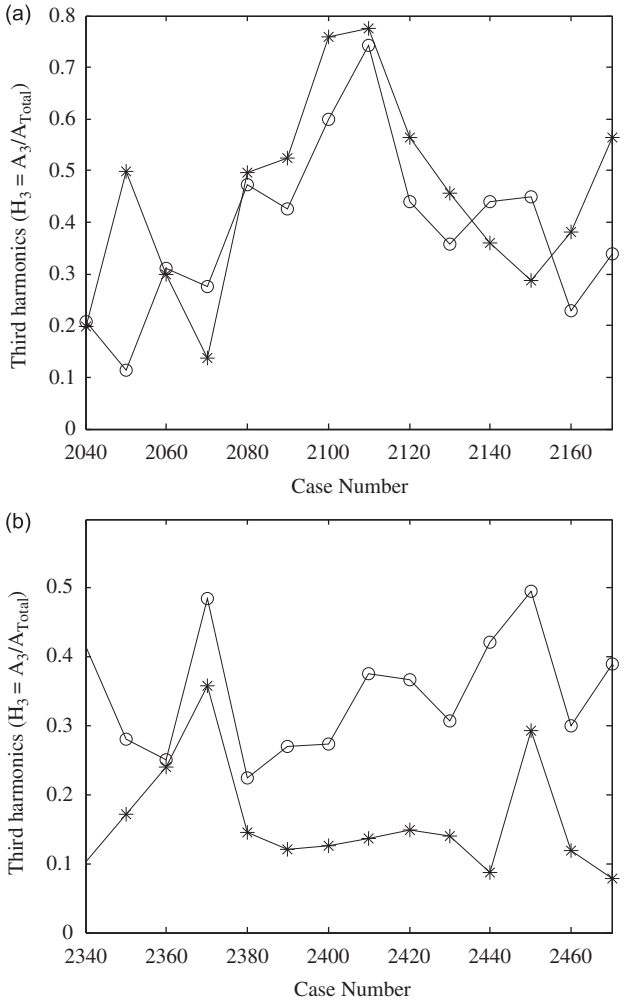

Fig. 10. Third harmonic components (H_3=A_3/A_{Total}, as defined in Section 4) of force signal at $z \sim 4$ m based on measured signals (∗) and predicted using the presented method (○) for (a) uniform flow cases (U=0.6 m/s for 2040 and 1.9 m/s for 2170) and (b) linearly sheared flow cases ($U_{\max}$=0.6 m/s for 2340 and 1.9 m/s for 2470).

8. Fatigue damage calculation

In order to calculate fatigue damage of the riser an S–N curve of the form $N=A(1/S)^B$ is used, where N is the number of cycles, S is stress in MPa, $A=4.8641\times10^{11}$ and $B=3.00$ [9]. Fatigue damage calculations are conducted based on rainflow fatigue prediction method (see, e.g. [12]).

Fatigue calculations can be conducted using the measured signals directly. Using the unfiltered signals, the most realistic fatigue damage can be calculated. These are shown by triangles in Fig. 11 for two sample cases of NDP data, the same cases as Figs. 8 and 9. Using the signals filtered around their fundamental frequency, a smaller fatigue damage is calculated (circles shown in Fig. 11), since the influence of higher harmonic components is not considered. These points can be compared with the continuous line which is fatigue damage calculated based on the reconstructed (and therefore purely first harmonic) signals. The limits due to uncertainties arising in reconstruction procedure are shown by thin lines. Once we have fatigue damage calculated using the purely first harmonic signal, we can use the following procedure in order to estimate a more realistic fatigue damage. We assume a worst case scenario in which the magnitude of the total stress is equal to the summation of the magnitudes of the stress due to each of the harmonics:

$$S_T = S_1 + S_3 + S_5, \tag{2}$$

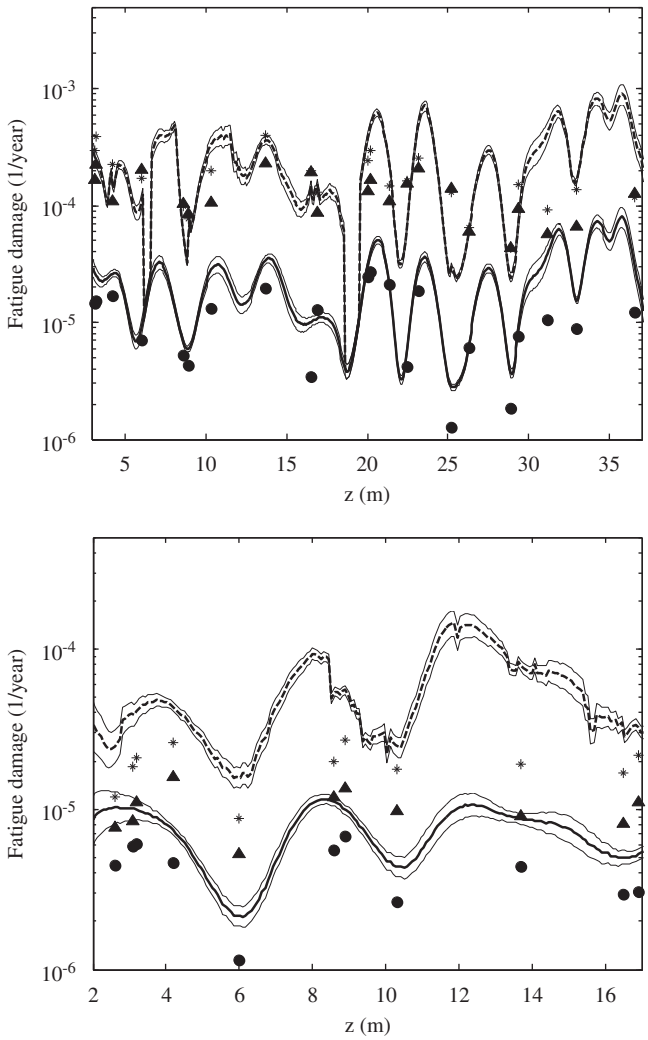

Fig. 11. Fatigue damage for NDP cases of (a) Fig. 8 and (b) Fig. 9. Values are calculated based on purely first harmonic reconstructed CF motion (continuous line), and based on first, third and fifth harmonics using higher harmonic predictions of the forced database (dashed line), while the thin lines correspond to the limits due to uncertainties arising in reconstruction procedure; direct fatigue calculations are conducted using the measured CF strain signals based on: only first harmonic (●); first, third and fifth harmonics (∗); and based on the unfiltered signal (▲).

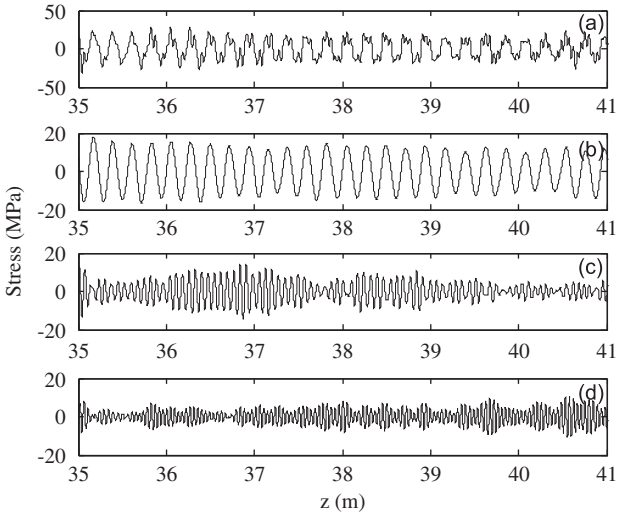

Fig. 12. (a) A sample stress function; (b) the signal filtered around its fundamental frequency (first harmonic component, f); (c) filtered around $3f$ (third harmonic component); and (d) filtered around $5f$ (fifth harmonic component).

or

$$S_T = S_1\left(1 + \left(\sqrt{H_3} + \sqrt{H_5}\right)/\sqrt{1 - H_3 - H_5}\right), \tag{3}$$

where S_1, S_3 and S_5 are magnitudes of the first, third and fifth harmonic stress, respectively, and are not function of time, and H_3 and H_5 are the higher harmonic components calculated using the unfiltered signals. Therefore the number of cycles to damage can be predicted as $N{=}A(1/S_T)^B$. The asterisks in Fig. 11 show the estimated fatigue damage following this procedure for the measured signals. These values can be compared relatively well with the damage predicted using the unfiltered signals. In Eq. (3) we assume that the amplitude of the third harmonic stress is equal to H_3 times the amplitude of the first harmonic stress, and H_3 is a time-averaged value over the entire time. However, it can be observed, e.g. from the stress signal and its harmonics shown in Fig. 12, that the ratio of these amplitudes changes with time, i.e. the amplitudes of the first and the third harmonics of stress signals are not necessarily correlated. The use of these time-averaged higher harmonic coefficients leads to the differences between estimated (asterisks) and actual (triangles) fatigue life values shown in Fig. 11. As an example, for the case of Fig. 12, the magnitude of the first harmonic stress is around 18 MPa, and the third and fifth harmonic components are calculated to be 0.3 and 0.2, respectively. Therefore, the magnitude of the total stress is predicted as

$$S_T = S_1\left(1 + \left(\sqrt{H_3} + \sqrt{H_5}\right)/\sqrt{1 - H_3 - H_5}\right) = 18\left(1 + \left(\sqrt{0.3} + \sqrt{0.2}\right)\Big/\sqrt{1 - 0.3 - 0.2}\right) = 43\,\text{MPa},$$

which is comparable with what is observed in Fig. 12(a).

This method can also be applied to the reconstructed response; in this case H_3 and H_5 are estimated using the rigid cylinder database. The dashed lines in Fig. 11 are the resulting fatigue damage calculations, while the thin lines around them show the limits due to uncertainties in the first-harmonic response reconstruction. It can be observed that the maximum fatigue damage is around $10^{-3}\,\text{years}^{-1}$ at $z \approx 35$ m for the uniform case of Fig. 11(a), while if one is limited to using the filtered signals and only at the measurement points, the maximum damage is calculated as $0.2 \times 10^{-4}\,\text{years}^{-1}$ at $z \approx 20$ m. The interesting fact about the predicted critical fatigue damage is that it occurs at a point where no measurement point is available ($z \approx 35$ m). Similar observation can be made for the linearly sheared case of Fig. 11(b). The critical fatigue damage is predicted as $2 \times 10^{-4}\,\text{years}^{-1}$ at $z \approx 12$ m, where the filtered measurement points would give $1 \times 10^{-5}\,\text{years}^{-1}$ at $z \approx 9$ m.

Fig. 13 shows the values of fatigue damage based on purely first harmonic oscillations divided by the fatigue damage predicted by taking into account the higher harmonic values, ($\text{Damage}_{\text{first harmonic}}/\text{Damage}_{\text{Real}}$), for 14 uniform and 14 sheared cases. It shows that: (i) the results we have shown for the two sample cases in Fig. 11 are representative of all NDP cases, and (ii) for all the cases the difference is around a factor of 10.

9. Conclusions

A method for estimating the fatigue life of marine risers continuously along the length of the riser is introduced as an initial stage of a useful tool for fatigue life estimation. The purpose of this method is to utilize measurements that exist in the field, without requiring any further instrumentation of risers and provide an estimation of fatigue life at points along

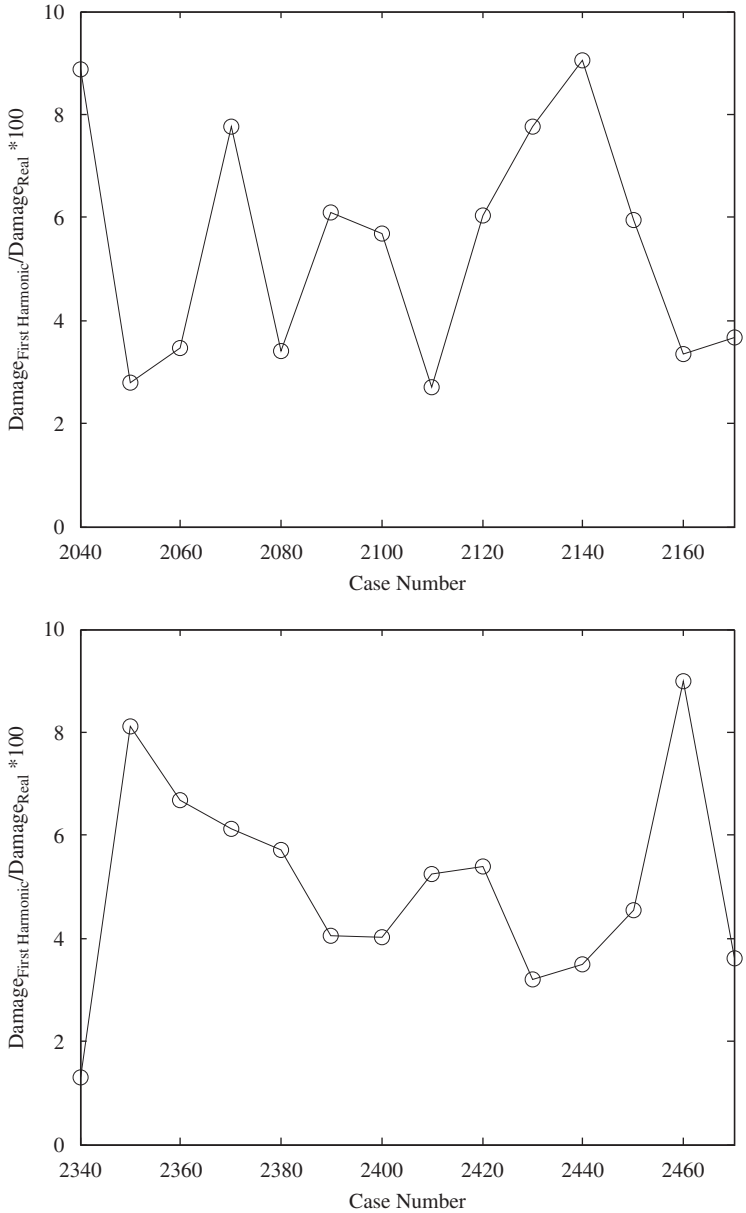

Fig. 13. Damage$_{\text{first harmonic}}$/Damage$_{\text{Real}} \times 100$ for (a) uniform flow cases (U=0.6 m/s for 2040 and 1.9 m/s for 2170) and (b) linearly sheared flow cases ($U_{\max}$=0.6 m/s for 2340 and 1.9 m/s for 2470).

the riser where measurements do or do not exist. Also, this method seeks to avoid a costly, full scale simulation of the coupled fluid and structure dynamics, in order to obtain a good estimate of fatigue life.

In the NDP experimental cases, which are used in this paper, higher harmonic components of strain and acceleration are significant. For the linearly sheared flow cases, the higher harmonics are of the order of 30–40 percent of total, while for the uniform flow cases they are around 50 percent of total. Counterclockwise figure-eight trajectories are noted at high flow regions of sheared flow cases; this region corresponds to the region under fluid excitation.

One essential assumption for the method used here is that a strip theory approach is applicable so as to use the 2-D database from experiments on rigid cylinders. In support of this assumption, we find that at the points where both strain and acceleration measurements are available there is good agreement between the higher harmonic components of force predicted using the forced rigid cylinder database and those directly calculated from the measured signals. This agreement is observed in majority of the NDP cases studied here, despite the errors due to a relatively sparse rigid cylinder database, the differences in Reynolds numbers in the experiments and the database as well as the assumptions related to the phase relationship between the components.

Also, in order to properly assess fatigue damage along the entire length of the riser, it is necessary to accurately reconstruct the riser response continuously along the span of the riser using the methodology introduced by Mukundan [10]. We estimate and show the effect of various uncertainties in this reconstruction method as an upper and lower bound of reconstructed motions, also reflected as error bounds on the calculated fatigue damage.

Fatigue damage calculations, based on a continuous reconstruction along the length and by taking into account the higher harmonic components, give fatigue damage values of one order of magnitude larger than those calculated based on only first harmonic signals and using data only from measurement points.

Acknowledgments

The authors acknowledge with gratitude the permission granted by the Norwegian Deepwater Programme (NDP) Riser and Mooring Project to use the Riser High Mode VIV tests. Support was provided by the BP-MIT Major Programs. The first author would like to acknowledge the financial support given to him from FQRNT.

References

[1] T. Sarpkaya, A critical review of the intrinsic nature of vortex-induced vibrations, *Journal of Fluids and Structures* 19 (2004) 389–447.
[2] C.H.K. Williamson, R. Govardhan, Vortex-induced vibrations, *Annual Review of Fluid Mechanics* 36 (2004) 413–455.
[3] J.K. Vandiver, Dimensionless parameters important to the prediction of vortex-induced vibration of long, flexible cylinders in ocean currents, *Journal of Fluids and Structures* 7 (1993) 423–455.
[4] N. Jauvtis, C.H.K. Williamson, The effect of two degrees of freedom on vortex-induced vibration at low mass and damping, *Journal of Fluid Mechanics* 509 (2004) 23–62.
[5] J.M. Dahl, F.S. Hover, M.S. Triantafyllou, S. Dong, G.E. Karniadakis, Resonant vibrations of bluff bodies cause multi-vortex shedding and high frequency forces, *Physical Review Letters* 99 (2007) 144503.
[6] S.B. Swithenbank, Dynamics of Long Flexible Cylinders at High-Mode Number in Uniform and Sheared Flows, Ph.D. Thesis, MIT, 2007.
[7] V. Jhingran, J.K. Vandiver, Incorporating the higher harmonics in VIV fatigue predictions, *Proceedings of the 26th International Conference on Offshore Mechanics and Arctic Engineering 2007, OMAE 2007*, 2007, pp. 891–899.
[8] H. Braaten, H. Lie, NDP riser high mode VIV tests, Main Report no. 512394.00.01, Norwegian Marine Technology Research Institute, 2004.
[9] A.D. Trim, H. Braaten, H. Lie, M.A. Tognarelli, Experimental investigation of vortex-induced vibration of long marine risers, *Journal of Fluids and Structures* 21 (2005) 335–361.
[10] H. Mukundan, Vortex Induced Vibration of Marine Risers: Motion and Force Reconstruction from Field and Experimental Data, Ph.D. Thesis, MIT, 2008.
[11] J.M. Dahl, Vortex Induced Vibrations of a Circular Cylinder with Combined In-line and Cross-flow Motions, Ph.D. Thesis, MIT, 2008.
[12] L. Christian, *Mechanical Vibration and Shock*, Vol. 4, Taylor & Francis, New York, NY, 2002.